J Infrared Milli Terahz Waves (2014) 35:432–444
DOI 10.1007/s10762-014-0060-5

On the Numerical Modeling of Terahertz Photoconductive Antennas

E. Moreno · M. F. Pantoja · F. G. Ruiz · J. B. Roldán · S. G. García

Received: 7 November 2013 / Accepted: 17 February 2014 /
Published online: 9 March 2014

Abstract This paper shows the relevance of mobility models to describe the carrier dynamics for the analysis of radiative semiconductor photoconductive devices in the terahertz regime. We have built a simulator that self-consistently solves the device physics and Maxwell's equations to study the radiated fields. In particular, we show a significant influence of an accurate description of the steady-state regime of the semiconductor device for calculating radiated electromagnetic fields in the broadside direction. Comparison with measurements shows the accuracy of our simulator and demonstrates the superior performance of numerical schemes based not only on the description of the carrier, electric potential, and field distributions, but also on reliable local mobility models.

Keywords Photoconductive antennas · Terahertz sources · Semiconductor device modeling

E. Moreno · M. F. Pantoja (✉) · S. G. García
Department of Electromagnetismo y Fisica de la Materia, Universidad de Granada, Granada 18071, Spain
e-mail: mario@ugr.es

E. Moreno
e-mail: emorenop@ugr.es

S. G. García
e-mail: salva@ugr.es

F. G. Ruiz · J. B. Roldán
Department of Electrónica, Universidad de Granada, Granada 18071, Spain

F. G. Ruiz
e-mail: franruiz@ugr.es

J. B. Roldán
e-mail: jroldan@ugr.es

1 Introduction

Recent years have brought renewed interest in the so-called terahertz regime, which is expected to make breakthroughs in spectroscopy and/or imaging in the near future [14]. These expectations are related mostly to the ability of the terahertz electromagnetic waves to interact with the vibrational and rotational modes of the matter, thus leading to the identification of molecules and compounds in any state. However, there is a lack of electron devices capable of operating efficiently in this regime, and present-day affordable sources are limited to providing power on the order of a few microwatts [4], which may be insufficient for the more demanding applications. Among all the sources available, the photoconductive antennas (PCAs) present drawbacks in terms of the supplied power, but they are widely used because of their low cost and relatively easy manufacture.

Initially proposed by Auston [2], PCAs are based on the radiation of electromagnetic energy by transient currents in semiconductors excited by a laser pulse. Experimental setups not only confirmed their performance in terahertz time-domain spectroscopy [7], but were also proposed as part of electro-optical controlled transistors [17]. The above-mentioned limitations of radiated power led to further effort to increase the efficiency of these devices, and several configurations of electrodes (stripline, dipole, and offset dipole) in different kinds of semiconductor alloys (e.g. low-temperature-grown GaAs and semi-insulating GaAs) were built and measured for comparison purposes [8, 26, 28]. Once the performance was shown to depend on the size, geometry, and materials of the PCA, it became a matter of interest to develop CAD software to decrease the design costs and achieve an optimal configuration. In this respect, many efforts have been devoted to assess numerically the emission properties of PCAs. Thus, a simple set of differential equations were formulated to describe effects such as the recombination of carriers and also the screening of the external electric field from photogenerated electron-hole pairs [5, 10, 18]. Another assumption of these approaches is the proportionality of the radiated field and the derivative of the current pulse [10, 18], which was also improved in [5] by incorporating a time-domain model of the electric field in terms of the current pulses [25]. These procedures achieve results showing a good agreement with experimental data. However, PCAs including asymmetric configurations of electrodes [3] and/or spatially dependent parameters (e.g., doping of substrate [30]) require full-wave procedures which are able to deal with steady-state distributions of fields and carriers at a prize of a more demanding computational burden.

Numerical simulation of semiconductor photoconductive devices at terahertz frequencies remains a challenge [1]. The main obstacle is the mixed nature of the problem, which involves a combination of electronic, electromagnetic, and optical phenomena [14]: a) the steady-state, corresponding to the initial distribution of electric fields, can be handled using well-known techniques in electronics to solve Poisson's equation inside the semiconductor [23, 32]; b) the non-equilibrium phase, accounting for the transient response of the system in terms of the description of the electric- and magnetic-field distributions in the device, is accomplished by finite-difference time-domain (FDTD) algorithms, broadly used by electromagnetic researchers [31]; and c) the focusing of electromagnetic radiation in the direction of

interest, in which optical procedures can help to design an additional lens for increasing the total efficiency, has to be dealt with [14]. Attempts to produce high-accuracy codes based on FDTD procedures have been presented with relative success, by proposing a modification of Yee's unit cell to consider the distribution of carriers in the semiconductor [9, 19, 20]. Following this line of research, some studies have extended the geometries and have incorporated drift-diffusion equations, which are computationally faster than approaches based on magnetohydrodynamic equations [6] or Monte-Carlo methods [16]. Nevertheless, as an initial approach, a homogeneous concentration of carriers in the steady-state of the PCA was assumed in some of the previous works referenced above, corresponding to that of the equilibrium for an intrinsic semiconductor. As we will show below, these assumptions lead to a lack of accuracy in the final radiated electric field in the broadside direction. At this point, the validity of the presented solver should be highlighted. Drift-diffusion model use is questionable for devices operating in large electric fields, high concentrations of carriers or timescales less than picoseconds [29]. Given these restrictions, THz devices (e.g. PCAs) under relatively low biasing voltages, with sizes on the order of micrometers [13], and net concentrations of carriers small enough to neglect the forces between charges [29] can be studied under the proposed numerical algorithm.

Apart from the presentation of the simulator we have developed, the main contribution of this paper is to show that the choice of numerical techniques and models to characterize the steady-state regime is key to achieving satisfactory results. In fact, despite that most of the computational time (roughly 95 %) is devoted to solving the coupled system of partial differential equations provided by the Maxwell equations and the drift-diffusion model, the accuracy in the description of steady-state regime proves decisive for accurately reproducing the physical phenomena inside the device. Consequently, it can be concluded that we need a new generation of numerical solvers for the terahertz regime [1], capable of integrating the numerical techniques used for the study of electron devices, as well as the characteristics within the realms of electromagnetics and optics. In fact, specialized CAD packages are lacking, and most of the numerical research in THz is produced by means of commercial electromagnetic or optical software tools. These tools avoid the time-consuming simulations required for accurately modeling the experimental set-ups by: a) approximating optical waveforms to perform the numerical link to the electromagnetic devices and/or b) applying physical optics equations. In this respect, this paper revisits the problem focusing on the relevance of providing an accurate description of the electron device steady-state regime (consisting of reliable electric potential and field as well as mobility distributions [12, 22]). In this manner, the sometimes neglected accuracy in the semiconductor steady-state description proves essential to reproduce PCA measurements.

2 Computational Semiconductor Model in the THz Regime

A typical PCA is the face-to-face (FF) dipole, depicted in Fig. 1. A biasing voltage is connected to a pair of electrodes, before applying an external pulse radiated by a femtosecond laser on the surface of the semiconductor. Thus, the stimulated electric

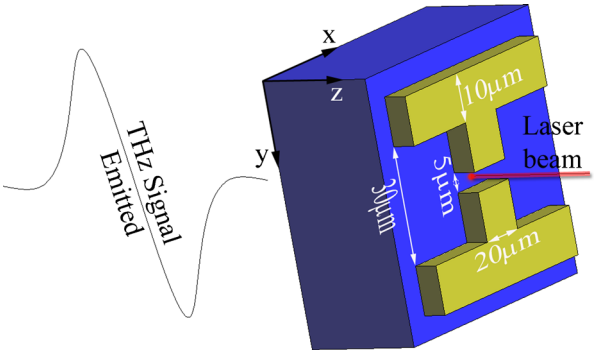

Fig. 1 Typical configuration of a face-to-face dipole photoconductive antenna. For representation purposes the figure is not scaled

carriers drift due to the biasing electric field, acting as sources of radiated electric and magnetic fields. The steady-state regime, once the biasing voltage is applied, can be described by Poisson and continuity equations. In particular, Poisson's equation can be written as follows:

$$\nabla \cdot (\nabla \phi (\mathbf{r})) = \frac{q}{\varepsilon} (n (\mathbf{r}) - p (\mathbf{r}) - C (\mathbf{r})) \tag{1}$$

where $C (\mathbf{r})$ stands for the fixed charge in the semiconductor, composed of singly ionized donors N_D^+ and acceptors N_A^-; $\phi (\mathbf{r})$ is the electric potential; and $n (\mathbf{r})$ and $p (\mathbf{r})$ are the electron and hole concentrations, respectively.

The continuity equations for both types of carriers can be expressed as:

$$\nabla \cdot [n (\mathbf{r}) \nabla \phi (\mathbf{r}) - V_T \nabla n (\mathbf{r})] = -\mu_n^{-1} (\mathbf{r}) R (\mathbf{r}) \tag{2}$$

$$\nabla \cdot [p (\mathbf{r}) \nabla \phi (\mathbf{r}) + V_T \nabla p (\mathbf{r})] = \mu_p^{-1} (\mathbf{r}) R (\mathbf{r}) \tag{3}$$

where μ_n, μ_p are the mobilities for electrons and holes, respectively; V_T corresponds to the thermal voltage; and $R (\mathbf{r})$ is the recombination rate function, which in this paper has been implemented by combining Shockley-Read-Hall and Auger models. The carrier concentrations and currents are achieved by the self-consistent solution of Eqs. 1–3.

For a proper modeling of the PCA, it should be taken into account that the high voltage applied to electrodes leads to significant electric fields in the semiconductor, which reduce the effective mobility. To take this effect into account, we use a parallel-field dependent mobility model [27]:

$$\mu_n (E) = 2\mu_{n_0} \left[1 + \left(1 + \left(\frac{2\mu_{n_0} E}{V_{sat,n}} \right)^{\beta_n} \right)^{\beta_n^{-1}} \right]^{-1} \tag{4}$$

$$\mu_p (E) = 2\mu_{p_0} \left[1 + \left(1 + \left(\frac{2\mu_{p_0} E}{V_{sat,p}} \right)^{\beta_p} \right)^{\beta_p^{-1}} \right]^{-1} \tag{5}$$

where E is the modulus of the parallel electric field and μ_{n_0} and μ_{p_0} are the low-field-electron and hole mobilities, respectively; β_n and β_p are parameters of the model, which depend of the semiconductor material, and the values of the saturation velocities of carriers $V_{sat,n}$ and $V_{sat,p}$ are taken as constants.

Unless a very dense grid is used, which will often lead to a computationally large problem, results based on a complete numerical finite-difference solution of Eqs. 1–3 will lead only to approximate results, due mostly to the non-linearity of the carrier distributions, which follow an exponential variation in certain areas [22]. In this respect, the consideration of truncated analytical solutions of the continuity equations in terms of Bernoulli functions enables an increased step size and higher accuracy in the solution [21].

Once steady-state regime is achieved, the impinging laser pulse generates pairs of electron-holes which are accelerated by the biasing electric field and the transient phase begins. A brief description of equations required in the simulation are given below. The transient electromagnetic fields $\mathbf{E}(\mathbf{r}, t)$ and $\mathbf{H}(\mathbf{r}, t)$ can be achieved by Ampere-Maxwell and Faraday equations:

$$\varepsilon \partial_t \mathbf{E}(\mathbf{r}, t) = \nabla \wedge \mathbf{H}(\mathbf{r}, t) - \mathbf{J}(\mathbf{r}, t) \tag{6}$$

$$\mu \partial_t \mathbf{H}(\mathbf{r}, t) = -\nabla \wedge \mathbf{E}(\mathbf{r}, t) \tag{7}$$

where μ is the magnetic permeability, and $\mathbf{J}(\mathbf{r}, t)$ is the total current density in the semiconductor. This current density is derived by adding the electron and hole components,

$$\mathbf{J}_n(\mathbf{r}, t) = q\mu_n(\mathbf{r})\left(n(\mathbf{r}, t)\mathbf{E}(\mathbf{r}, t) + V_T \nabla n(\mathbf{r}, t)\right) \tag{8}$$

$$\mathbf{J}_p(\mathbf{r}, t) = q\mu_p(\mathbf{r})\left(p(\mathbf{r}, t)\mathbf{E}(\mathbf{r}, t) - V_T \nabla p(\mathbf{r}, t)\right) \tag{9}$$

Finally, the carrier dynamics included in Eqs. 8 and 9 are calculated by the continuity charge equations:

$$\partial_t n(\mathbf{r}, t) = -RG(\mathbf{r}, t) + q^{-1}\nabla \cdot \mathbf{J}_n(\mathbf{r}, t) \tag{10}$$

$$\partial_t p(\mathbf{r}, t) = -RG(\mathbf{r}, t) - q^{-1}\nabla \cdot \mathbf{J}_p(\mathbf{r}, t) \tag{11}$$

where $RG(\mathbf{r}, t) = R(\mathbf{r}, t) - G(\mathbf{r}, t)$ is the net rate of recombination which accounts for carrier generation-recombination in the semiconductor.

3 Results

To show the relevance of the steady-state description for calculating radiated electromagnetic fields, we consider the LT-GaAs ($\varepsilon_r = 13.26$) PCA-FF dipole of Fig. 1 [26]. The bias voltage was assumed to be 30 V and the doping concentration $N_D = 10^{16}\ cm^{-3}$. The parameters of the mobility model used were $\mu_{n_0} = 8000\ \frac{cm^2}{V \cdot s}$ and $\mu_{p_0} = 400\ \frac{cm^2}{V \cdot s}$. Here, time-domain results are used to validate the numerical method and obtain the main results. Time-domain solvers present advantages over frequency-domain ones in terms of computational time when the broadband description is considered, which is the usual case in applications such as THz spectroscopy. Also, they provide useful information about the physical phenomena involved, in this

case through the carrier-dynamics modeling. However, the matching of experimental and simulated responses is more challenging in time-domain graphs, and therefore the validation in the THz regime is often presented solely in the frequency-domain [11].

Following the approach described in Section 2, a solution in the steady-state operation regime led to the distributions of electric potential and electrons at the semiconductor surface shown in Figs. 2 and 3 (which are consistent with those provided by commercial software [24]). Although these figures are not new for electron devices, some features deserve to be highlighted in order to indicate their importance within the THz regime context. On one hand, the distribution of the electrostatic potential between the electrodes needs to be accurately described (Fig. 2) because the laser spot—usually circular or elliptical—can be beamed at any zone of the upper surface. Consequently, the possible screening and non-linear effects disable any analytical approach that might be used to approximate the steady-state regime of the electric-field distribution. As long as this field contributes to the total current density, $\mathbf{J}(\mathbf{r}, t)$, the transient THz waveform will be strongly affected by inaccuracies at this stage. On the other hand, the carrier distribution is also key for the transient electromagnetic-field calculation, because Eqs. are 8 and 9 inserted in Eqs. 10 and 11 at each timestep, and the steady-state regime initial distribution strongly affects the complete solution. Moreover, it is difficult to estimate the peaky surface distribution of carriers at the metallic contact tips (see Fig. 3), and previous proposed approaches based on the assumption of equilibrium carrier distributions greatly differ from the real one. In this sense, for certain cases (e.g. a FF-dipole excited by a small laser spot centered in the nearest region of electrodes or a strip-line dipole with a

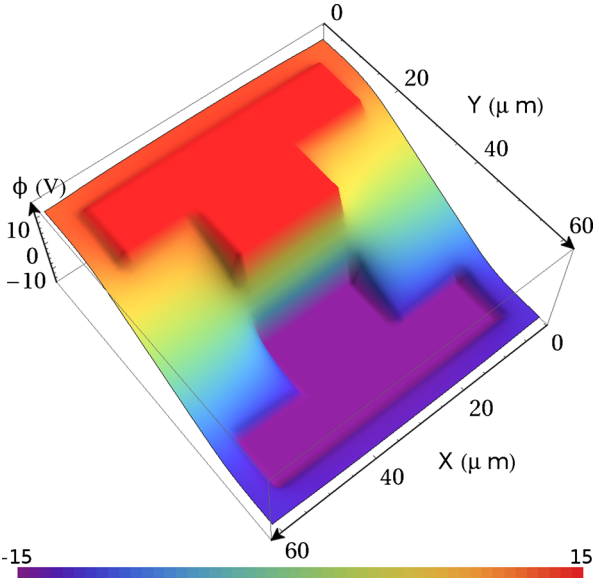

Fig. 2 Electric potential at the interface between semiconductor and electrodes in the steady-state regime

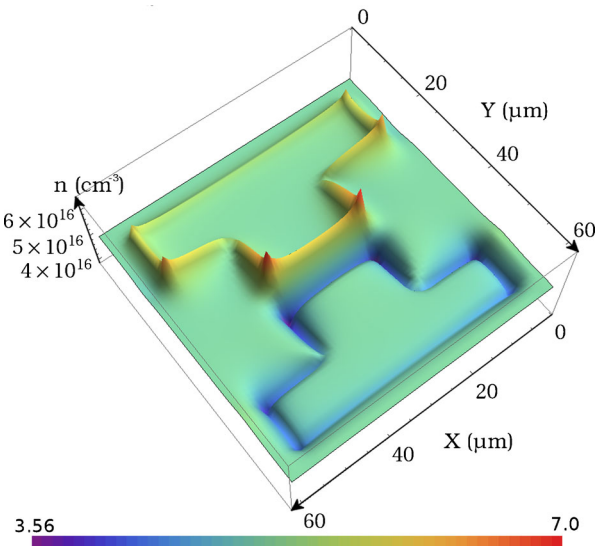

Fig. 3 Steady-state electron distribution at the interface between semiconductor and electrodes (a doping concentration $N_D = 7.5 \cdot 10^{16} cm^{-3}$ is used to enhance the accumulation of charge)

laser source just below the central part of the electrode [14]), the steady-state regime may be described by considering equilibrium carrier distributions and a linear dependence for the electrostatic potential, which means a constant electrostatic field at the laser spot area. However, for more complex geometrical electrode configurations, a detailed electrical device solver (self-consistently coupled with an electromagnetic solver) is needed.

Furthermore, special attention should be paid to the non-homogeneous mobility distribution (a field-dependent model has been used here [24, 27]) at the steady-state regime. The choice of the particular model may depend on the material, field distribution, geometry of the electrodes, etc.. Results of this paper have been derived for the FF-dipole. Initially, the influence on the radiated field of a particular mobility model cannot be assessed (more on this issue below); nevertheless, as Fig. 4 depicts, differences of one order of magnitude can be found within the mobility-value distribution. Also, in contrast to the carrier distribution, the mobility-time dependence can be neglected because the biasing electric field is much larger than the transient electric-field, and thus the mobility does not need to be recalculated for each time-step. Four different models were considered in our approach using: a) a homogeneous mobility model, which is inadequate to reproduce the experimental data; b) a first parallel model, following Eqs. 4 and 5 with choices of $\beta_n = 1.82$ and $\beta_p = 1.75$; c) a second parallel model (accounting only for the electric field projection in the main current direction) corresponding to the Caughey-Thomas mobility model [13, 24], with $\beta_n = \beta_p = 2$; and d) the Lombardi-CVT volumetric model [15], which accounts for the mobility of carriers inside the inversion layers. Details of the mobility-model implementations for b), c), and d) can be found in [13, 24, 27], respectively.

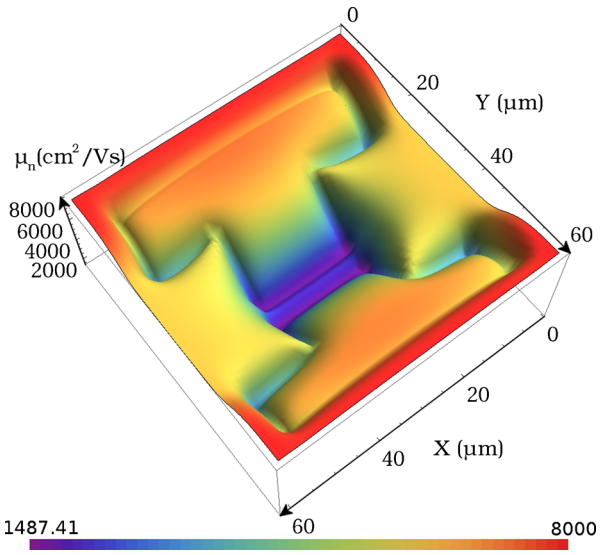

Fig. 4 Field-dependent mobility at the interface between semiconductor and electrodes at the steady-state regime

For the transient solution, the modeling of parameters such as the recombination rate is key for the THz regime description. Here it is employed a Shockley-Read-Hall (SRH) model with an electron and hole lifetime of $\tau_n = 0.3\ ps$ and $\tau_p = 0.4\ ps$, respectively. The incoming laser beam [26] impinges at the surface of the semiconductor at (x_0, y_0, z_0), centered in the inner part of electrodes (Fig. 1), with an optical intensity of $I_0 = 0.5\ W/\mu m^2$ and a wavelength $\lambda_\gamma = 780\,nm$. The generation of carriers at any point (x, y, z) is given by the function G:

$$G(\mathbf{r}, t) = G_0 \left(1 - e^{-\alpha_\lambda |z - z_0|}\right) h(x, y, z, t) \tag{12}$$

where $G_0 = \frac{I_0 \lambda_\gamma \alpha_\lambda T \xi}{hc}$ is the peak generation rate, which includes the parameters α_λ as the photonic absorption coefficient (taken as $1\ \mu m^{-1}$ in the simulations), $T = 0.8$ as the transmittance in the vacuum-semiconductor interface and $\xi = 0.9$ as the rate of pairs (e-h) which contribute to the total electric current. The function $h(x, y, z, t)$ accounts for the spatial distribution of carriers in the form:

$$h(x, y, z, t) = e^{-\left(\left(\frac{|x - x_0|}{\sigma_x}\right)^2 + \left(\frac{|y - y_0|}{\sigma_y}\right)^2 + \left(\frac{t - t_0 - \frac{|z - z_0| n_\lambda}{c}}{\sigma_t}\right)^2 + \alpha_\lambda |z - z_0|\right)} \tag{13}$$

where $\sigma_x = 1.8\ \mu m$, $\sigma_y = 1.8\ \mu m$, $\sigma_t = 80\ fs$ describe the spatial and temporal distribution of the spot laser, $n_\lambda = 3.68$ corresponds to the refractive index of the semiconductor and $t_0 = 4.2\ ps$ is a reference time.

Figure 5 depicts the time-domain Gaussian waveform of the incoming laser pulse formerly described. The current rise time, and consequently the local electromagnetic field, follows the incoming pulse, as it is shown by lines depicting the current

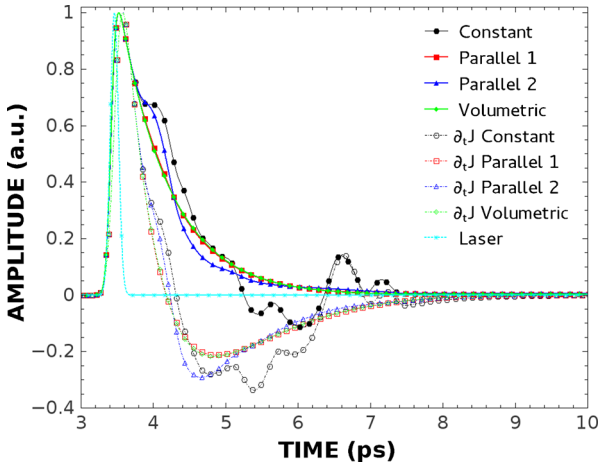

Fig. 5 Time-domain current pulses, and derivative of the current pulses, at the center of the spot. Also, time-domain laser source waveform (wavelength: $\lambda_\gamma = 780$ nm; pulse width: $\sigma_t = 80$ fs) [26] is depicted as reference

density at the top of the semiconductor, just at the center of the laser spot. However, the decay time works in a different way. It is governed mainly by the carrier recombination rate, and regardless of the decay rate of the incident pulse, the current density remains appreciable. It can be also observed the key role played in the decay time by each mobility model: unrealistic late-time reflections appear for high mobilities such as those employed in the constant model or the second parallel model. Finally, time-derivative currents are also included as a reference for a further comparison of radiated fields. In Fig. 6, the spectrum of the pulses of Fig. 5 are depicted. The laser source, with a bandwidth which ranges up to roughly 10 THz, is limited in bandwidth up to the 2–3 THz for the pulses corresponding to densities of current. Those currents act as source of the electromagnetic radiation, which also presents this narrower

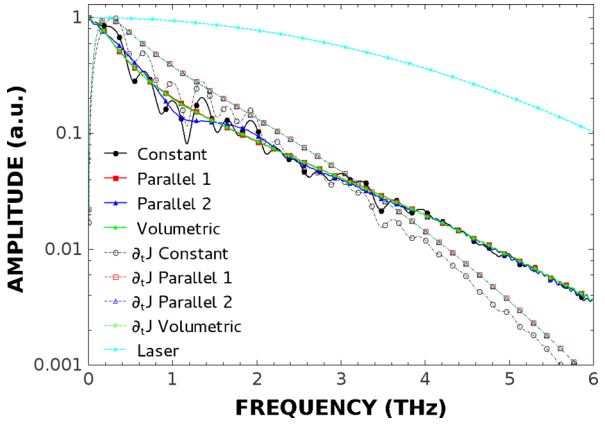

Fig. 6 Frequency-domain pulses corresponding to currents and derivative of currents at the center of the spot, and also to the laser source pulse

bandwidth as reported experimentally [26]. Thus we conclude that an adequate estimation of the recombination rate for our experimental sample is crucial to reproduce the experimental measurements in practice.

Figures 7 and 8 depict the radiated electrical field obtained with numerical simulations and also the experimental measurements for comparison. In this case, the dependence of the final results on the mobility model is emphasized. The electron device and electromagnetic solvers were coupled in order to reproduce the experimentally measured radiation electric field [26] in the broadside direction (shown as $-Z$ in Fig. 1). To this end, it is applied the approach presented in [18] to calculate the detected pulse from the radiated field at broadside direction. Thus, Fig. 7 reflects that the choice of mobility model affects the final simulation result. An initial approach based on the homogeneous mobility causes oscillations due to electromagnetic reflections coming from the boundaries, which require of a total travel time of roughly 2 ps to reach the end points of the PCA. This unrealistic homogeneous approach has been included to illustrate the relevance of mobility models in order to produce satisfactory results, because solutions at time-steps higher than twice the time needed to travel the minimum dimension of the device are inaccurate. This issue has dramatic consequences in the frequency-domain solution (Fig. 8). Thus, results from non-homogeneous mobility models are also considered. In this respect, any of the parallel or volumetric models could be deemed valid when only the frequency-domain graphs are considered. The time-domain graph provides a better estimation of the effect of the more realistic mobility models, i.e. the volumetric or first-parallel model, which fit the experimental data. The first-parallel model improves the referenced second-parallel because of the more realistic description of the characteristics of LT-GaAs substrate with the parameters ($\beta_n = 1.82$, $\beta_p = 1.75$), according to [24]. However, the more detailed Lombardi-CVT volumetric model does not offer a better match of the experimental response. The main reason for this lack of improvement is the electrostatic field distribution in the PCA, which is parallel to the surface of the semiconductor. Thus the parallel-mobility models offer an adequate numerical

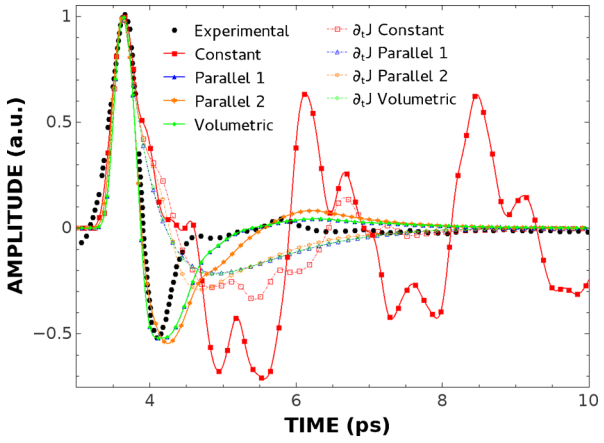

Fig. 7 Time-domain detected pulse from radiated electric fields in the broadside direction

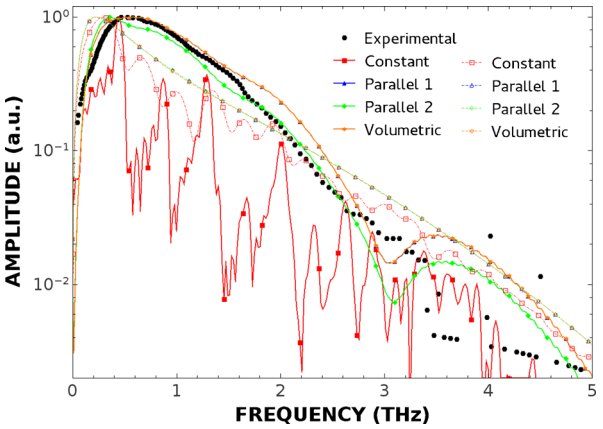

Fig. 8 Frequency-domain detected pulse from radiated electric fields in the broadside direction

description with lower computational demands compared to the volumetric mobility models. Another noteworthy issue is the discrepancy in the 1.5–2.5 THz of Fig. 8 for both models. In this case, the accurate steady-state description is inadequate to reproduce the experimental results, and other numerical issues, such as the above-mentioned limitations of the drift-diffusion model or the numerical modeling of the THz system, may be the origin of these differences. Regarding the derivative of the current pulses, Fig. 8 confirms the reasonable accuracy of the models based on partial differential equations. This fact is noticeable taking into account the negligible computational burden required, and also suggests the employment of such equations in those cases where simplifying assumptions are hold.

In any case, better results are achieved when implementing proper considerations regarding realistic physical models. As pointed out in the Introduction, these results are notable since more than 95 % of the computational time is devoted to solving Maxwell and drift-diffusion equations for any of these descriptions. Therefore, the improvement comes from an accurate initial description of the magnitudes characterizing the steady-state regime of the electron device. Although it is clear that better final results are expected when higher accuracy is employed in the physical models, we analyze the improvement quantitatively and in detail. This issue is not trivial since several authors have built their simulation codes using approximations whose consequences have been clarified here. In addition, our simulation infrastructure, developed from scratch, has allowed us to delve more deeply into time- and frequency-domain analysis.

4 Conclusion

This paper has shown that an accurate simulation description of photoconductive antennas from the device level is required to match experimental measurements involving these devices in the electromagnetic context. Despite being governed

mainly by electromagnetic-radiation parameters, PCA modeling requires not only an accurate description of the carrier dynamics but also a realistic description of the initial steady-state regime in terms of carrier, electric potential and field distributions, and an accurate field-dependent local mobility model in the semiconductor. The results demonstrate the superior performance of the hybrid electronic-electromagnetic numerical technique intended to model devices in the THz operation regime. Experimental data have been accurately reproduced both in the time and frequency domains. Advances improving accuracy in electron device numerical simulations are of great relevance in THz electronics, where researchers can find an appropriate scenario to test state-of-the-art numerical methods both in the electromagnetics and electron device realms.

Acknowledgments This work was supported in part by the Spanish Ministry of Education under Project CSD2008-00068, the Junta de Andalucia Project P09-TIC-5327, the EU FP7/2007-2013, under grant 205294 (HIRF-SE project), and the Spanish National Project TEC2010-20841-C04-04.

References

1. Armstrong, C.: The truth about terahertz. Spectrum, IEEE **49**(9), 36–41 (2012)
2. Auston, D.H., Nuss, M.C.: Electrooptical generation and detection of femtosecond electrical transients **24**(2), 184–197 (1988)
3. Cai, Y., Brener, I., Lopata, J., Wynn, J., Pfeiffer, L., Federici, J.: Design and performance of singular electric field terahertz photoconducting antennas. Appl Phys Lett **71**(15), 2076–2078 (1997)
4. Eisele, H.: State of the art and future of electronic sources at terahertz frequencies. Electronics Letters **46**(26), S8–S11 (2010)
5. Ezdi, K., Heinen, B., Jrdens, C., Vieweg, N., Krumbholz, N., Wilk, R., Mikulics, M., Koch, M.: A hybrid time-domain model for pulsed terahertz dipole antennas. Journal of the European Optical Society - Rapid publications **4**(0) (2009)
6. Goldston, R.J., Rutherford, P.H.: Introduction to plasma physics. CRC Press (2010)
7. Grischkowsky, D., Katzenellenbogen, N.: Femtosecond pulses of terahertz radiation: physics and applications. OSA Proceedings on Picosecond Electronics and Optoelectronics **9** (1991)
8. Hou, L., Shi, W.: An lt-GaAs terahertz photoconductive antenna with high emission power, low noise, and good stability **60**(5), 1619–1624 (2013)
9. Hughes, S., Tani, M., Sakai, K.: Vector analysis of terahertz transients generated by photoconductive antennas in near- and far-field regimes. Journal of Applied Physics **93**(8), 4880–4884 (2003)
10. Jepsen, P.U., Jacobsen, R.H., Keiding, S.R.: Generation and detection of terahertz pulses from biased semiconductor antennas. J. Opt. Soc. Am. B **13**(11), 2424–2436 (1996)
11. Khabiri, M., Neshat, M., Safavi-Naeini, S.: Hybrid computational simulation and study of continuous wave terahertz photomixers. IEEE Transactions on Terahertz Science and Technology **2**(6), 605–616 (2012)
12. Kim, D.M., Song, S.H., Baek, K.H., Kim, D.J., Kim, H.J.: Microwave characteristics of a pseudomorphic high electron mobility transistor under electro-optical stimulations **21**(3), 93–96 (2000)
13. Kirawanich, P., Yakura, S., Islam, N.: Study of high-power wideband terahertz-pulse generation using integrated high-speed photoconductive semiconductor switches. Plasma Science, IEEE Transactions on **37**(1), 219–228 (2009)
14. Lee, Y.S.: Principles of Terahertz Science and Technology. Springer (2009)
15. Lombardi, C., Manzini, S., Saporito, A., Vanzi, M.: A physically based mobility model for numerical simulation of nonplanar devices. Computer-Aided Design of Integrated Circuits and Systems, IEEE Transactions on **7**(11), 1164–1171 (1988)
16. Lundstrom, M.: Fundamentals of carrier transport. Cambridge University Press (2009)
17. Morse, J.D., Mariella R. P., J., Anderson, G.D., Dutton, R.W.: Picosecond optoelectronic gating of silicon bipolar transistors by locally integrated gaas photoconductive devices **12**(7), 379–381 (1991)

18. Piao, Z., Tani, M., Sakai, K.: Carrier dynamics and terahertz radiation in photoconductive antennas. Japanese Journal of Applied Physics **39**(Part 1, No. 1), 96–100 (2000)
19. Reineix, A., Ariaudo, M., Chatenet, C., Jecko, B.: Theoretical analysis of photoconducting dipole antennas. Microwave and Optical Technology Letters **15**(2), 110–113 (1997)
20. Sano, E., Shibata, T.: Fullwave analysis of picosecond photoconductive switches **26**(2), 372–377 (1990)
21. Scharfetter, D.L., Gummel, H.K.: Large-signal analysis of a silicon read diode oscillator **16**(1), 64–77 (1969)
22. Selberherr, S.: Analysis and Simulation of Semiconductor Devices. Springer-Verlag (1984)
23. Shen, C., Ong, S.L., Heng, C.H., Samudra, G., Yeo, Y.C.: A variational approach to the two-dimensional nonlinear poisson's equation for the modeling of tunneling transistors **29**(11), 1252–1255 (2008)
24. SILVACO International: ATLAS User's Manual: Device Simulation Software (2010)
25. Smith, G.S.: An Introduction to Classical Electromagnetic Radiation. Cambridge University Press (1997)
26. Tani, M., Matsuura, S., Sakai, K., Nakashima, S.: Emission characteristics of photoconductive antennas based on low-temperature-grown GaAs and semi-insulating GaAs. Appl. Opt. **36**(30), 7853–7859 (1997)
27. Technische Universitat Wien, Austria: MINIMOS-NT 2.1 User's Guide (2004)
28. Wang, B., Zhang, T., Liu, K., Qiu, J.: Characteristics of the GaAs photoconductive semiconductor switch operated in linear-alike mode **60**(8), 2580–2585 (2013)
29. Willis, K., Hagness, S., Knezevic, I.: Multiphysics simulation of high-frequency carrier dynamics in conductive materials. Journal of Applied Physics **110**(6), 063,714–063,714 (2011)
30. Xu, L., Zhang, X.C., Auston, D., Jalali, B.: Terahertz radiation from large aperture Si p-i-n diodes. Applied Physics Letters **59**(26), 3357–3359 (1991)
31. Yee, K.: Numerical solution of initial boundary value problems involving maxwell's equations in isotropic media **14**(3), 302–307 (1966)
32. Zandler, G., Di Carlo, A., Kometer, K., Lugli, P., Vogl, P., Gornik, E.: A comparison of monte carlo and cellular automata approaches for semiconductor device simulation **14**(2), 77–79 (1993)